

The following resources related to this article are available online at www.sciencemag.org (this information is current as of July 6, 2009):

Updated information and services, including high-resolution figures, can be found in the online version of this article at:

<http://www.sciencemag.org/cgi/content/full/309/5734/600>

This article **cites 40 articles**, 10 of which can be accessed for free:

<http://www.sciencemag.org/cgi/content/full/309/5734/600#otherarticles>

This article has been **cited by** 125 article(s) on the ISI Web of Science.

This article has been **cited by** 27 articles hosted by HighWire Press; see:

<http://www.sciencemag.org/cgi/content/full/309/5734/600#otherarticles>

This article appears in the following **subject collections**:

Atmospheric Science

<http://www.sciencemag.org/cgi/collection/atmos>

Information about obtaining **reprints** of this article or about obtaining **permission to reproduce this article** in whole or in part can be found at:

<http://www.sciencemag.org/about/permissions.dtl>

numbers CZ551658 to CZ552046. We thank members of the Rubin and Pääbo laboratories for insightful discussions and support. This work was performed under the auspices of the U.S. Department of Energy's Office of Science Biological and Environmental Research Program and by the University of California; Lawrence Berkeley National Laboratory; Lawrence Livermore National Laboratory; and Los Alamos Na-

tional Laboratory under contract numbers DE-AC03-76SF00098, W-7405-Eng-48, and W-7405-ENG-36, respectively, with support from NIH grants U1 HL66681B and T32 HL07279 and at the Max Planck Institute for Evolutionary Anthropology.

Supporting Online Material
www.sciencemag.org/cgi/content/full/1113485/DC1

Materials and Methods
Tables S1 to S3
References

12 April 2005; accepted 26 May 2005
Published online 2 June 2005;
10.1126/science.1113485
Include this information when citing this paper.

Marked Decline in Atmospheric Carbon Dioxide Concentrations During the Paleogene

Mark Pagani,¹ James C. Zachos,² Katherine H. Freeman,³
Brett Tipple,¹ Stephen Bohaty²

The relation between the partial pressure of atmospheric carbon dioxide ($p\text{CO}_2$) and Paleogene climate is poorly resolved. We used stable carbon isotopic values of di-unsaturated alkenones extracted from deep sea cores to reconstruct $p\text{CO}_2$ from the middle Eocene to the late Oligocene (~45 to 25 million years ago). Our results demonstrate that $p\text{CO}_2$ ranged between 1000 to 1500 parts per million by volume in the middle to late Eocene, then decreased in several steps during the Oligocene, and reached modern levels by the latest Oligocene. The fall in $p\text{CO}_2$ likely allowed for a critical expansion of ice sheets on Antarctica and promoted conditions that forced the onset of terrestrial C_4 photosynthesis.

The early Eocene [~52 to 55 million years ago (Ma)] climate was the warmest of the past 65 million years. Mean annual continental temperatures were considerably elevated relative to those of today, and high latitudes were ice-free, with polar winter temperatures ~10°C warmer than at present (1–3). After this climatic optimum, surface- and bottom-water temperatures steadily cooled over ~20 million of years (4, 5), interrupted by at least one major ephemeral warming in the late middle Eocene (6). High-latitude cooling eventually sustained small Antarctic ice sheets by the late Eocene (7), culminating in a striking climate shift across the Eocene/Oligocene boundary (E/O) at 33.7 Ma. The E/O climate transition, Earth's first clear step into "icehouse" conditions during the Cenozoic, is associated with a rapid expansion of large continental ice sheets on Antarctica (8, 9) in less than ~350,000 years (10, 11).

Changes in the partial pressure of atmospheric carbon dioxide ($p\text{CO}_2$) are largely credited for the evolution of global climates during the Cenozoic (12–14). However, the relation between $p\text{CO}_2$ and the extraordinary climate history of the Paleogene is poorly constrained. Initial attempts to estimate early Paleogene $p\text{CO}_2$ have provided conflicting results, with both high (15) and low (i.e., similar to modern) (16) estimates of $p\text{CO}_2$. This

deficiency in our understanding of the history of $p\text{CO}_2$ is critical, because the role of CO_2 in forcing long-term climate change during some intervals of Earth's history is equivocal. For example, Miocene $p\text{CO}_2$ records (~25 to 5 Ma) argue for a decoupling between global climate and CO_2 (15–17). These records suggest that Miocene $p\text{CO}_2$ was rather low and invariant across periods of both inferred global warming and high-latitude cooling (17). Clearly, a more complete understanding of the relation between $p\text{CO}_2$ and climate change requires the extension of paleo- $p\text{CO}_2$ records back into periods when Earth was substantially warmer and ice-free.

Paleoatmospheric CO_2 concentrations can be estimated from the stable carbon isotopic compositions of sedimentary organic molecules known as alkenones. Alkenones are long-chained (C_{37} – C_{39}) unsaturated ethyl and methyl ketones produced by a few species of Haptophyte algae in the modern ocean (18). Alkenone-based $p\text{CO}_2$ estimates derive from records of the carbon isotopic fractionation that occurred during marine photosynthetic carbon fixation (ϵ_p). Chemostat experiments conducted under nitrate-limited conditions indicate that alkenone-based ϵ_p values ($\epsilon_{p37:2}$) vary as a function of the concentration of aqueous CO_2 ($[\text{CO}_{2\text{aq}}]$) and specific growth rate (19–21). These experiments also provide evidence that cell geometry accounts for differences in ϵ_p among marine microalgae cultured under similar conditions (21). In contrast, results from dilute batch cultures conducted under nutrient-replete conditions yield substantially lower $\epsilon_{p37:2}$ values, a different relation for ϵ_p versus

$\mu/\text{CO}_{2\text{aq}}$ (where μ = algal growth rate), and a minimal response to $[\text{CO}_{2\text{aq}}]$ (22). Thus, comparison of the available culture data suggests that different growth and environmental conditions potentially trigger different carbon uptake pathways and carbon isotopic responses (23). A recent evaluation of the efficacy of the alkenone- CO_2 approach, using sedimentary alkenones in the natural environment, supported the capacity of the technique to resolve relatively small differences in water column $[\text{CO}_{2\text{aq}}]$ across a variety of marine environments when phosphate concentrations and temperatures are constrained (24).

In our study, we extended records of the carbon isotopic composition of sedimentary alkenones ($\delta^{13}\text{C}_{37:2}$) from the middle Eocene to the late Oligocene and established a record of $p\text{CO}_2$ for the past ~45 million years. Samples from Deep Sea Drilling Project sites 516, 511, 513, and 612 and Ocean Drilling Program site 803 (Fig. 1) were used to reconstruct $\delta^{13}\text{C}_{37:2}$ and $\epsilon_{p37:2}$ records ranging from the middle Eocene to the late Oligocene (~25 to 45 Ma). These sites presumably represent a range of oceanic environments with a variety of surface-water nutrient and algal-growth conditions and thus reflect a set of environmental and physiological factors affecting both $\delta^{13}\text{C}_{37:2}$ and $\epsilon_{p37:2}$ values.

These data are presented as a composite record, in large part because the measurable concentration of di-unsaturated alkenones varied both spatially and temporally. Moreover, continuous alkenone records spanning the entire Eocene and Oligocene from individual sites were not recovered. As a consequence, most of the Oligocene record is represented at site 516, whereas the majority of the Eocene is represented at site 612 (Fig. 2A). Age models for each site were developed by linearly interpolating between biostratigraphic datums (25–31), calibrated to the Geomagnetic Polarization Time Scale (32).

Eocene $\delta^{13}\text{C}_{37:2}$ values range from ~–30 to –35 per mil (‰), with the most negative values (sites 511 and 513) occurring near the E/O boundary. $\delta^{13}\text{C}_{37:2}$ values increase substantially through the Oligocene with maximum values of ~–27‰ by ~25.5 Ma. This trend is briefly reversed near the end of the Oligocene as $\delta^{13}\text{C}_{37:2}$ values become more negative, reaching ~–32‰ by 25 Ma (Fig. 2A). The overall pattern of ^{13}C enrichment continues into the Miocene, establishing a clear secular trend from the middle Eocene to the middle Miocene (Fig. 2B). These isotopic

¹Department of Geology and Geophysics, Yale University, 210 Whitney Avenue, New Haven, CT 06511, USA.

²Earth Sciences Department, University of California, 1156 High Street, Santa Cruz, CA 95064, USA. ³Department of Geosciences, Pennsylvania State University, University Park, PA 16802, USA.

trends do not mirror changes in the $\delta^{13}\text{C}$ of dissolved inorganic carbon ($\delta^{13}\text{C}_{\text{DIC}}$) because $\delta^{13}\text{C}$ records of bulk carbonate (33) and benthic foraminifera (10) indicate small changes in $\delta^{13}\text{C}_{\text{DIC}}$ for the Eocene to Oligocene relative to the change in $\delta^{13}\text{C}_{37:2}$. Nonetheless, interpretations of long-term trends in $\delta^{13}\text{C}_{37:2}$ are enhanced when $\delta^{13}\text{C}_{37:2}$ values are converted to $\epsilon_{\text{p}37:2}$ (34), thus eliminating the influence of $\delta^{13}\text{C}_{\text{DIC}}$.

The temporal pattern of $\epsilon_{\text{p}37:2}$ is similar to that of $\delta^{13}\text{C}_{37:2}$ (Fig. 2, C and D), consistent with other studies (17). Higher values of $\epsilon_{\text{p}37:2}$ (~19.5 to 21.5‰) characterize the Eocene and then decrease through the Oligocene. The $\epsilon_{\text{p}37:2}$ values recorded for the Eocene and earliest Oligocene are higher than any recorded for the modern ocean (Fig. 2D). Given our present understanding of the controls on $\epsilon_{\text{p}37:2}$, the decrease in $\epsilon_{\text{p}37:2}$ from the Eocene through the Oligocene could be driven by a consistent change in the cell dimensions of alkenone-producing algae over time, a secular increase in growth rates of alkenone-producing algae, or a long-term decrease in $[\text{CO}_{2\text{aq}}]$ and/or increased utilization of bicarbonate ($[\text{HCO}_3^-]$) as a result of low $[\text{CO}_{2\text{aq}}]$ (35). At present, evolutionary changes in algal cell geometries are poorly constrained. If the long-term decrease in $\epsilon_{\text{p}37:2}$ were driven solely by changes in algal cell dimensions, it would require a pattern of increasing ratios of cell volume to surface area with time. If ϵ_{p} scales linearly with the ratio of cell volume to surface area (21), the observed change in $\epsilon_{\text{p}37:2}$ values would require an ~60% increase in the cell diameters of alkenone-producing algae from the Eocene to the Miocene (i.e., sites 516 and 612). Further, given that Miocene and Modern $\epsilon_{\text{p}37:2}$ values are similar, Eocene coccolithophores would have to have been ~60% smaller than modern alkenone producers, such as *Emiliania huxleyi*, with cell diameters of ~5 μm (21). However, the available data suggest that placoliths from probable alkenone producers, specifically species within the genus *Reticulofenestra*, were substantially larger than modern species and then decreased through the Oligocene and early Miocene (36, 37). If we reasonably assume that placolith geometry scales to cell geometry (38), then cell diameters decreased during the late Paleogene. A trend of decreasing cell diameters should lead to an increase in $\epsilon_{\text{p}37:2}$ values (21), which is contrary to our measurements. Thus, although a long-term change in cell geometry might have influenced the relative magnitude of Paleogene $\epsilon_{\text{p}37:2}$ values, it was not responsible for the pattern observed in our record.

Alternatively, variations in $\epsilon_{\text{p}37:2}$ could be ascribed to variations in the specific growth rates of alkenone-producing algae (μ_{alk}), with higher μ_{alk} values associated with lower $\epsilon_{\text{p}37:2}$ values. Under this scenario, Eocene and early

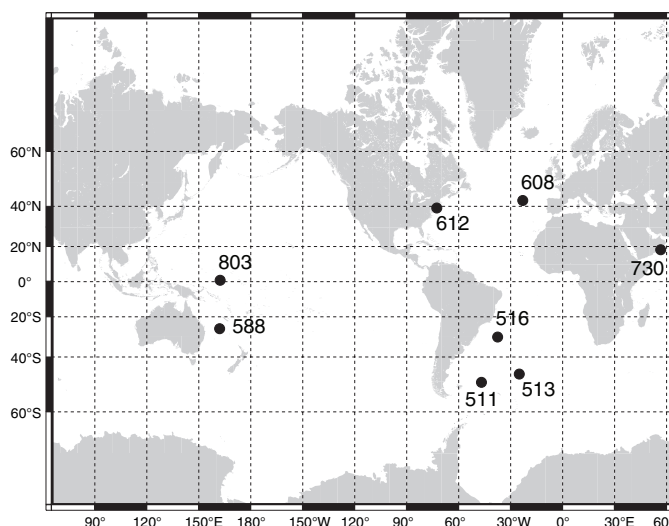


Fig. 1. Site location map. Sites 612, 516, 803, 511, and 513 were used to reconstruct Eocene and Oligocene $\epsilon_{\text{p}37:2}$ values. Sites 588, 608, 730, and 516 were used to reconstruct Miocene $\epsilon_{\text{p}37:2}$ values.

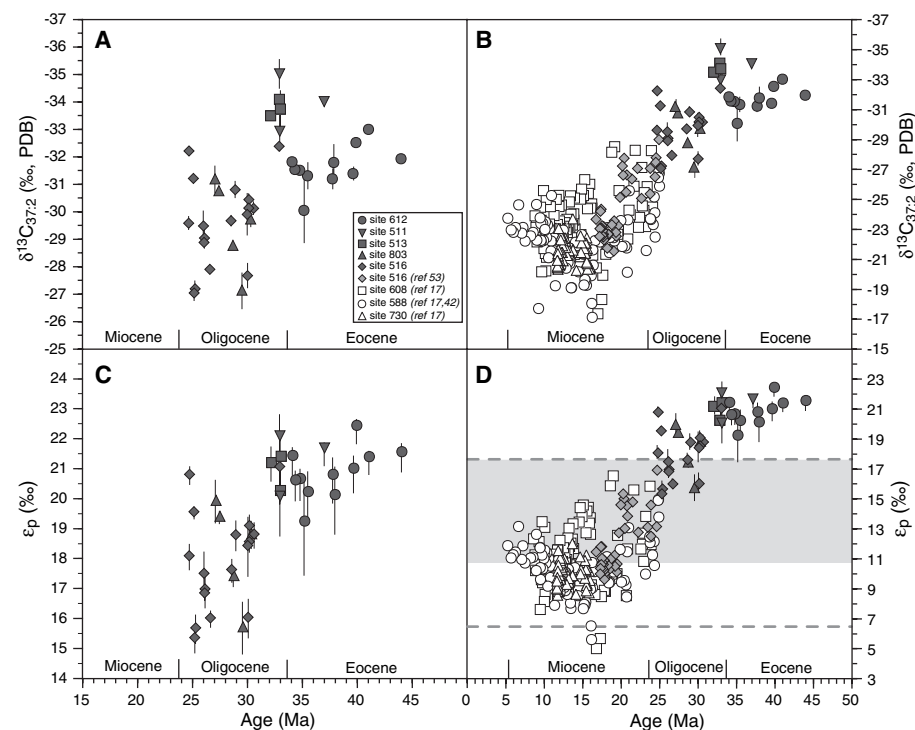


Fig. 2. (A) Stable carbon isotopic composition of di-unsaturated alkenones. Each data point represents one measurement or an average of multiple measurements, with error bars bracketing the range of values for each sample. PDB, Pee Dee belemnite standard. (B) Compilation of the carbon isotopic composition of di-unsaturated alkenones from this study and Pagani *et al.* (17, 42, 53). (C) Paleogene $\epsilon_{\text{p}37:2}$ values. $\epsilon_{\text{p}37:2}$ is calculated from the $\delta^{13}\text{C}$ of di-unsaturated alkenones as follows: $\epsilon_{\text{p}37:2} = [(\delta d + 1000/\delta p + 1000) - 1] \times 10^3$, where δd is the carbon isotopic composition of $\text{CO}_{2\text{aq}}$ calculated from mixed-layer carbonates and δp is the carbon isotopic composition of haptophyte organic matter enriched by 4.2‰ relative to alkenone $\delta^{13}\text{C}$ (54). Carbon isotopic compositions of mixed-layer carbonates were used to calculate δd by assuming equilibrium conditions and applying temperature-dependent isotope equations (55, 56). Mixed-layer temperatures were calculated from the $\delta^{18}\text{O}$ of planktonic foraminifera (57) as follows: site 612, *Acarinina* spp.; site 513, *Subbotina* spp. and *Chiloguembelina cubensis*; and site 511, *Subbotina* spp. Temperatures for sites 516 and 803 were estimated from the $\delta^{18}\text{O}$ compositions of the <60- μm carbonate fraction, assuming that the $\delta^{18}\text{O}$ composition of seawater changed from -0.75‰ during the Eocene to -0.5‰ during the Oligocene. Error bars reflect the range of $\epsilon_{\text{p}37:2}$ values calculated by applying the maxima and minima of both the measured $\delta^{13}\text{C}$ of di-unsaturated alkenones and calculated temperatures. (D) Compilation of $\epsilon_{\text{p}37:2}$ values from this study and Pagani *et al.* (17, 42, 53). Dashed horizontal lines bracket the range of $\epsilon_{\text{p}37:2}$ values from surface waters of modern oceans. In general, higher and lower $\epsilon_{\text{p}37:2}$ values come from oligotrophic and eutrophic environments, respectively. The shaded box represents the range of $\epsilon_{\text{p}37:2}$ values from oligotrophic sites where $[\text{PO}_4^{3-}]$ ranges between 0.0 to 0.2 $\mu\text{mol/liter}$.

Oligocene $\epsilon_{p37.2}$ values must reflect substantially lower μ_{alk} than modern μ_{alk} found in oligotrophic waters where $[PO_4^{3-}]$ is $\sim 0.3 \mu\text{mol/liter}$ (Fig. 2D). That is, algal growth rates during the Paleogene from both eutrophic and oligotrophic environments would have to be lower than the lowest growth rates found in the modern oligotrophic ocean. Further, if growth rates were indeed the first-order control on $\epsilon_{p37.2}$ values, the lowest Miocene $\epsilon_{p37.2}$ values would require substantially higher algal growth rates in oligotrophic settings, comparable to those of the highly productive Peru upwelling margin (Fig. 2D). Therefore, we conclude that

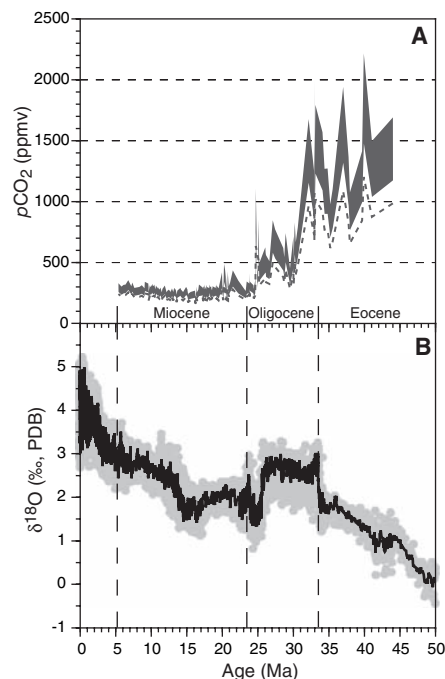


Fig. 3. (A) $p\text{CO}_2$ estimates calculated from $\epsilon_{p37.2}$. $\epsilon_p = \epsilon_f - b/[\text{CO}_{2aq}]$ (39), where $b = \{(118.52[\text{PO}_4^{3-}] + 84.07)/(25 - \epsilon_{p37.2})\}$, calculated from the geometric mean regression of all available data (19, 20, 23, 58, 59). $[\text{CO}_{2aq}]$ values were calculated using mean $\epsilon_{p37.2}$ values and a range of $[\text{PO}_4^{3-}]$ values for each site. $[\text{PO}_4^{3-}]$ ranges applied for individual sites were as follows: site 612, 0.5 to 0.3 $\mu\text{mol/liter}$; site 516, 0.4 to 0.2 $\mu\text{mol/liter}$; sites 511 and 513, 1.10 to 0.8 $\mu\text{mol/liter}$; site 803, 0.3 to 0.1 $\mu\text{mol/liter}$; and site 588, 0.3 to 0.2 $\mu\text{mol/liter}$. Values of CO_{2aq} were converted to $p\text{CO}_2$ by applying Henry's Law (60), calculated assuming a salinity of 35 and surface-water temperatures derived from $\delta^{18}\text{O}$ of marine carbonates. Maximum $p\text{CO}_2$ estimates were calculated using maximum temperatures (61) for each sample and maximum $[\text{PO}_4^{3-}]$ for each site. Intermediate and minimum (dashed line) $p\text{CO}_2$ estimates were calculated using intermediate and minimum temperatures for each sample and minimum $[\text{PO}_4^{3-}]$ for each site. An analytical treatment of error propagation suggests that relative uncertainties in reconstructed CO_2 values are $\sim 20\%$ for the Miocene data and approach 30 to 40% for Paleogene samples with higher (20 to 24‰) $\epsilon_{p37.2}$ values (62). (B) Global compilation of benthic oxygen isotope records (5).

rather extraordinary changes in μ_{alk} are required to explain the temporal pattern of $\epsilon_{p37.2}$ values and thus are not the primary cause for the observed long-term trends. Instead, we contend that the Cenozoic evolution of $\epsilon_{p37.2}$ was forced primarily by changes in $[\text{CO}_{2aq}]$ and $p\text{CO}_2$. Accordingly, these records would qualitatively reflect high surface-water $[\text{CO}_{2aq}]$ during the middle to late Eocene, a pattern of decreasing $[\text{CO}_{2aq}]$ through the Oligocene, and near-modern levels during the Neogene. If the change in $\epsilon_{p37.2}$ values during the Paleogene was brought about by an increased utilization of HCO_3^- over CO_{2aq} , then it implies that $[\text{CO}_{2aq}]$ became increasingly limiting to algal growth in both oligotrophic and eutrophic environments. Although this would compromise quantitative estimates of atmospheric $p\text{CO}_2$, it would still support a scenario of decreasing $p\text{CO}_2$ with time. Until evidence emerges to the contrary, we must assume that the physiological processes responsible for $\epsilon_{p37.2}$ in the past were similar to those operating in modern surface waters (19, 24) and use these data to estimate both $[\text{CO}_{2aq}]$ and $p\text{CO}_2$ over the past 45 million years.

The conversion of $\epsilon_{p37.2}$ values to $p\text{CO}_2$ requires an estimate of surface-water $[\text{PO}_4^{3-}]$ (39) and temperature for each site. For this study, we assumed that modern surface-water distributions of $[\text{PO}_4^{3-}]$ at each site between 0 and 100 m encompassed the probable range at any given time, and we applied temperatures derived from the oxygen isotope composition of coeval carbonates in order to convert estimates of $[\text{CO}_{2aq}]$ to $p\text{CO}_2$. This approach assumes relative air-sea equilibrium, which may not be valid for every site. However, although disequilibrium could lead to overestimates of $p\text{CO}_2$, our treatment of the data ultimately yields a range of CO_2 concentrations that reflects the uncertainty associated with this effect. On a broad scale, our results indicate that CO_2 concentrations during the middle to late Eocene ranged between 1000 and 1500 parts per million by volume (ppmv) (40) and then rapidly decreased during the Oligocene, reaching modern levels by the latest Oligocene (Fig. 3A). In detail, a trend toward lower CO_2 concentrations is evident from the middle to late Eocene, reaching levels by the E/O boundary that could have triggered the rapid expansion of ice on east Antarctica (2). An episode of higher $p\text{CO}_2$ in the latest Oligocene occurs concomitantly with a ~ 2 -million-year low in the mean $\delta^{18}\text{O}$ composition of benthic foraminifera (Fig. 3B), indicating that global climate and the carbon cycle were linked from the Eocene to the late Oligocene. This association weakens in the Neogene, when long-term patterns of climate and $p\text{CO}_2$ appear to be decoupled (17).

In addition to climate, the change in CO_2 implied by our record would have substantially affected the growth characteristics of ter-

restrial flora. In particular, the expansion of C_4 grasses has received considerable attention as an indicator of environmental change (41, 42). The C_4 pathway concentrates CO_2 at the site of carboxylation and enhances rates of photosynthesis by eliminating the effects of photorespiration under low CO_2 concentrations (43). Moreover, higher rates of carbon assimilation can be maintained under water-stressed conditions. This results in a water-use efficiency (water loss per unit of carbon assimilated) in C_4 plants that is twice that of C_3 plants at $\sim 25^\circ\text{C}$ (44). Given our understanding of the environmental parameters affecting C_3 and C_4 plants, a prevalent supposition has emerged that C_4 photosynthesis originated as a response to stresses associated with photorespiration (41, 45). The CO_2 threshold below which C_4 photosynthesis is favored over C_3 flora is estimated at ~ 500 ppmv (41), a level that is breached during the Oligocene. Molecular phylogenies (46, 47) and isotopic data (48) place the origin of C_4 grasses before the Miocene between 25 to 32 Ma (46, 47, 49), the interval when CO_2 concentrations approached modern levels. This confluence strongly suggests that C_4 photosynthesis evolved as a response to increased photorespiration rates forced by a substantial drop in $p\text{CO}_2$ during the Oligocene. Near-global expansion of C_4 ecosystems ensued later in the Miocene (41), possibly driven by drier climates and/or changes in patterns of precipitation (42).

References and Notes

- J. C. Zachos, L. D. Stott, K. C. Lohmann, *Paleoceanography* **9**, 353 (1994).
- K. G. Miller, R. G. Fairbanks, G. S. Mountain, *Paleoceanography* **2**, 1 (1987).
- L. D. Stott, J. P. Kennett, N. J. Shackleton, *Proc. Ocean Drilling Program Sci. Results* **113**, 849 (1990).
- N. J. Shackleton, J. P. Kennett, *Init. Rep. Deep Sea Drill. Proj.* **29**, 743 (1975).
- J. C. Zachos, M. Pagani, L. Sloan, E. Thomas, K. Billups, *Science* **292**, 686 (2001).
- S. Bohaty, J. C. Zachos, *Geology* **31**, 1017 (2003).
- J. V. Browning, K. G. Miller, D. K. Pak, *Geology* **24**, 639 (1996).
- C. Robert, J. P. Kennett, *Geology* **25**, 587 (1997).
- J. C. Zachos, B. N. Opdyke, C. N. Quinn, C. E. Jones, A. N. Halliday, *Chem. Geol.* **161**, 165 (1999).
- J. C. Zachos, T. M. Quinn, K. A. Salamy, *Paleoceanography* **11**, 251 (1996).
- H. K. Coxall, P. A. Wilson, H. Pälike, C. H. Le, *Nature* **433**, 53 (2005).
- M. E. Raymo, *Geology* **19**, 344 (1991).
- R. A. Berner, Z. Kothavala, *Am. J. Sci.* **301**, 182 (2001).
- R. M. DeConto, D. Pollard, *Nature* **421**, 245 (2003).
- P. N. Pearson, M. R. Palmer, *Nature* **406**, 695 (2000).
- D. L. Royer et al., *Nature* **292**, 2310 (2001).
- M. Pagani, M. A. Arthur, K. H. Freeman, *Paleoceanography* **14**, 273 (1999).
- M. H. Conte, J. K. Volkman, G. Eglinton, in *The Haptophyte Algae*, J. C. Green, B. S. C. Leadbeater, Eds. (Clarendon Press, Oxford, 1994), pp. 351–377.
- R. R. Bidigare et al., *Global Biogeochem. Cycles* **11**, 279 (1997).
- R. R. Bidigare et al., *Global Biogeochem. Cycles* **13**, 251 (1999).
- B. N. Popp et al., *Geochim. Cosmochim. Acta* **62**, 69 (1998).
- U. Riebesell, A. T. Revill, D. G. Hodsworth, J. K. Volkman, *Geochim. Cosmochim. Acta* **64**, 4179 (2000).
- E. A. Laws, B. N. Popp, R. R. Bidigare, *Geochim. Geophys. Geosyst.* **2**, 2000GC000057 (2001).

24. M. Pagani, K. H. Freeman, N. Ohkouchi, K. Caldeira, *Paleoceanography* **17**, 1069 (2002).
25. P. Valentine, *Init. Rep. Deep Sea Drill. Proj.* **95**, 359 (1987).
26. K. G. Miller, W. A. Berggren, J. Zhang, J. A. A. Palmer, *Palaios* **6**, 17 (1991).
27. W. Wei, S. W. Wise, *Mar. Micropaleontol.* **14**, 119 (1989).
28. C. Pujol, *Init. Rep. Deep Sea Drill. Proj.* **72**, 623 (1983).
29. R. M. Leckie, C. Farnham, M. G. Schmidt, *Proc. Ocean Drill. Program* **130**, 113 (1993).
30. S. W. Wise Jr., *Init. Rep. Deep Sea Drill. Proj.* **71**, 481 (1983).
31. I. A. Basov, P. F. Ciesielski, V. A. Krashenninikov, F. M. Weaver, S. W. Wise Jr., *Init. Rep. Deep Sea Drill. Proj.* **71**, 445 (1983).
32. W. A. Berggren, D. V. Kent, C. C. I. Swisher, M. P. Aubry, in *Geochronology, Time Scales and Global Stratigraphic Correlation*, W. A. Berggren, D. V. Kent, M. P. Aubry, J. Hardenbol, Eds. (Special Publication No. 54, Society for Sedimentary Geology, Tulsa, OK, 1995), pp. 129–212.
33. N. J. Shackleton, M. A. Hall, A. Boersma, *Init. Rep. Deep Sea Drill. Proj.* **74**, 599 (1984).
34. Calculation of $\epsilon_{p37.2}$ requires knowledge of the $\delta^{13}\text{C}$ of ambient $\text{CO}_{2\text{aq}}$ ($\delta^{13}\text{C}_{\text{CO}_{2\text{aq}}}$) during alkenone production and of temperature, which can be approximated from the $\delta^{13}\text{C}$ of shallow-dwelling foraminifera, assuming isotopic and chemical equilibria among all the aqueous inorganic carbon species and atmospheric CO_2 , as well as foraminiferal calcite (17). In this study, records of planktonic foraminifera coeval with alkenone measurements were available from sites 511, 513, and 803. Site 612 had well-preserved planktonic and benthic foraminifera, but some samples lacked coeval samples of planktonic foraminifera. In these cases, the isotopic compositions of planktonic foraminifera were modeled by calculating the average difference between benthic and planktonic foraminifera and adding this value to the isotopic compositions of benthic foraminifera. Site 516 had poor carbonate preservation and lacked an adequate foraminiferal record. For this site, surface $\delta^{13}\text{C}_{\text{CO}_{2\text{aq}}}$ and values were modeled from the $\delta^{13}\text{C}$ compositions of the <60- μm fine fraction (FF), assuming an isotopic offset between the FF and shallow-dwelling foraminifera of $+0.5\text{‰}$, as indicated by Miocene (50) and Eocene (this study) records from this site. Similarly, surface-water temperatures, required in the calculation of both $\delta^{13}\text{C}_{\text{CO}_{2\text{aq}}}$ and $p\text{CO}_2$, were estimated from the $\delta^{18}\text{O}$ compositions of shallow-dwelling planktonic foraminifera or modeled from the $\delta^{18}\text{O}$ compositions of the <60 μm FF, assuming an isotopic offset between the FF and shallow-dwelling foraminifera of -1.5‰ (50).
35. B. Rost, U. Riebesell, S. Burkhardt, *Limnol. Oceanogr.* **48**, 55 (2003).
36. J. Backman, J. O. R. Hermelin, *Palaeogeogr. Palaeoclimatol. Palaeoecol.* **57**, 103 (1986).
37. J. Young, *J. Micropaleontol.* **9**, 71 (1990).
38. J. Young, personal communication.
39. $\epsilon_{p37.2}$ is related to $[\text{CO}_{2\text{aq}}]$ by the expression $\epsilon_p = \epsilon_f - b/[\text{CO}_{2\text{aq}}]$, where ϵ_f represents the carbon isotope fractionation due to carboxylation. b represents the sum of physiological factors, such as growth rate and cell geometry, affecting the total carbon isotope discrimination. In the modern ocean, b is highly correlated to surface-water $[\text{PO}_4^{3-}]$ (19). However, it is unlikely that $[\text{PO}_4^{3-}]$ alone is responsible for the variability in growth rate inferred from variation in b . Instead, $[\text{PO}_4^{3-}]$ may represent a proxy for other growth-limiting nutrients, such as specific trace elements that exhibit phosphate-like distributions.
40. For comparison with our record, middle to late Eocene estimates of ocean pH using the boron isotopic compositions of foraminifera (15) yield early Eocene CO_2 concentrations that are potentially 10 times higher than preindustrial levels (~ 3500 ppmv), reaching levels as low as ~ 350 ppmv during the middle to late Eocene. Our Eocene estimates do not support a scenario of low $p\text{CO}_2$ during this time.
41. T. E. Cerling *et al.*, *Nature* **389**, 153 (1997).
42. M. Pagani, K. H. Freeman, M. A. Arthur, *Science* **285**, 876 (1999).
43. R. W. Pearcy, J. Ehleringer, *Plant Popul. Biol.* **7**, 1 (1984).
44. M. D. Hatch, *Biochim. Biophys. Acta* **895**, 81 (1987).
45. J. R. Ehleringer, R. F. Sage, L. B. Flanagan, R. W. Pearcy, *Trends Ecol. Evol.* **6**, 95 (1991).
46. B. S. Gaut, J. F. Doebley, *Proc. Natl. Acad. Sci. U.S.A.* **94**, 6809 (1997).
47. E. A. Kellogg, in *C₄ Plant Biology*, R. F. Sage, R. K. Monson, Eds. (Academic Press, New York, 1999), pp. 313–371.
48. D. L. Fox, P. L. Koch, *Geology* **31**, 809 (2003).
49. R. E. Sage, *New Phytol.* **161**, 341 (2004).
50. A. Ennyu, M. A. Arthur, M. Pagani, *Mar. Micropaleontol.* **46**, 317 (2002).
51. D. P. Schrag, *Chem. Geol.* **161**, 215 (1999).
52. P. N. Pearson *et al.*, *Nature* **413**, 481 (2001).
53. M. Pagani, M. A. Arthur, K. H. Freeman, *Paleoceanography* **15**, 486 (2000).
54. B. N. Popp, F. Kenig, S. G. Wakeham, E. A. Laws, R. R. Bidigare, *Paleoceanography* **13**, 35 (1998).
55. W. G. Mook, J. C. Bommerson, W. H. Staberman, *Earth Planet. Sci. Lett.* **22**, 169 (1974).
56. C. S. Romanek, E. L. Grossman, J. W. Morse, *Geochim. Cosmochim. Acta* **56**, 419 (1992).
57. J. Erez, B. Luz, *Geochim. Cosmochim. Acta* **47**, 1025 (1983).
58. B. N. Popp *et al.*, in *Reconstructing Ocean History: A Window into the Future*, F. Abrantes, A. Mix, Eds. (Plenum, New York, 1999), pp. 381–398.
59. M. E. Eek, M. J. Whiticar, J. K. B. Bishops, C. S. Wong, *Deep-Sea Res. II* **46**, 2863 (1999).
60. R. F. Weiss, *Mar. Chem.* **2**, 203 (1974).
61. All carbonates are assumed to be diagenetically altered to some degree, which acts to increase their $\delta^{18}\text{O}$ composition (51, 52), yielding minimum temperatures. In order to compensate for this uncertainty, three temperature estimates were used in the calculation of $\epsilon_{p37.2}$ and $p\text{CO}_2$, reflecting minimum temperatures calculated directly from the $\delta^{18}\text{O}$ value of carbonates (Temp_{min}), intermediate temperatures ($\text{Temp}_{\text{min}} + 3^\circ\text{C}$), and maximum temperatures ($\text{Temp}_{\text{min}} + 6^\circ\text{C}$).
62. K. H. Freeman, M. Pagani, in *A History of Atmospheric CO_2 and its Effects on Plants, Animals, and Ecosystems*, J. R. Ehleringer, T. E. Cerling, M. D. Dearing, Eds. (Springer, New York, 2005), pp. 35–61.
63. The authors thank two anonymous reviewers who helped improve the quality of the manuscript. We also thank B. Berner and K. Turekian for coffee and animated conversations that helped develop and inspire ideas. This work was funded by a grant from NSF.

21 January 2005; accepted 7 June 2005

Published online 16 June 2005;

10.1126/science.1110063

Include this information when citing this paper.

Global Mammal Conservation: What Must We Manage?

Gerardo Ceballos,^{1*} Paul R. Ehrlich,² Jorge Soberón,^{3†} Irma Salazar,¹ John P. Fay²

We present a global conservation analysis for an entire “flagship” taxon, land mammals. A combination of rarity, anthropogenic impacts, and political endemism has put about a quarter of terrestrial mammal species, and a larger fraction of their populations, at risk of extinction. A new global database and complementarity analysis for selecting priority areas for conservation shows that $\sim 11\%$ of Earth’s land surface should be managed for conservation to preserve at least 10% of terrestrial mammal geographic ranges. Different approaches, from protection (or establishment) of reserves to countryside biogeographic enhancement of human-dominated landscapes, will be required to approach this minimal goal.

Research on population and species extinctions shows an accelerating decay of contemporary biodiversity. This pressing environmental problem is likely to become even worse in coming decades (1–3). Although impacts of human activities are global in scope, they are not uniformly distributed. The biota of certain countries and regions can be identified as being most at risk, having both exceptionally high

richness and endemism and exceptionally rapid rates of anthropogenic change. Because resources for conservation are limited, ecologists must provide managers and politicians with solid bases for establishing conservation priorities (4) to minimize population and species extinctions (5), to reduce conservation conflicts (6, 7), and to preserve ecosystem services (8).

Even for charismatic taxa, we lack a global view of patterns of species distributions useful for establishing conservation priorities. Such a view would allow evaluation of the effort required, for example, to preserve all species in a given taxon. It would also be relevant to setting global conservation goals such as protecting a certain percentage of Earth’s land surface (9). More restricted approaches such as identifying hot spots and endemic bird areas have called attention to relatively small areas where large numbers of species might be protected (10–13). For instance, recently the number of vertebrate species that lack populations within major protected areas was estimated (12). But now more comprehensive analyses are possible.

¹Instituto de Ecología, UNAM, Apdo. Postal 70-275, México D.F. 04510, México. ²Center for Conservation Biology, Department of Biological Sciences, Stanford University, Stanford, CA 94305–5020, USA. ³Comisión Nacional de Biodiversidad, Periferico-Insurgentes 4903, Mexico.

*To whom correspondence should be addressed. E-mail: gceballo@miranda.ecologia.unam.mx

†Present address: Natural History Museum, Dyke Hall, University of Kansas, Lawrence, KS 66045, USA.